/CDF/ANAL/TOP/CDFR/8866
June 18, 2007

Measurement of W-Boson Helicity Fractions in Top-Quark Decays Using $\cos\theta^*$

Shulamit Moed (Harvard)
R. Eusebi, D.Glenzinski, A.Hocker (Fermilab)

June 18, 2007

We present a measurement of the fraction of longitudinally (f_0) and right-handed (f_+) polarized W bosons produced in top-quark decays through an analysis of the $\cos\theta^*$ distribution in $t\bar{t}$ candidate events using fully reconstructed lepton plus jets events. This analysis is based on a total integrated luminosity of 1530 pb^{-1}. We find $f_0 = 0.51 \pm 0.12 \pm 0.04$ with f_+ fixed to zero, and $f_+ = -0.07 \pm 0.04 \pm 0.025$ with f_0 fixed to the Standard Model expectation of 0.70. We determine $f_+ < 0.06$ at 95% CL.
We then simultaneously fit for the longitudinal and the right-handed fractions and find $f_0 = 0.58 \pm 0.24 \pm 0.036$ and $f_+ = -0.04 \pm 0.10 \pm 0.034$.

Contents

1 Introduction

An important consequence of the large mass of the top quark is that it decays in good approximation as a free quark. Its expected lifetime is $\approx 0.5 \times 10^{-24}$s and it therefore decays about an order of magnitude faster than the time needed to form a bound state with other quarks. As a consequence, the spin information carried by the top quark is preserved in the decay products. The underlying dynamics can be studied with minimal impact from gluon radiation and binding effects of QCD.

Studies of decay angular distributions provide a direct probe of the V − A nature of the Wtb coupling of the longitudinal and transverse polarized W bosons to the top quark. In the Standard Model, the fraction of decays to longitudinally polarized W bosons is determined by the masses of the involved particles and is expected to be [1-3]

$$f_0 = \frac{\Gamma(W_0)}{\Gamma(W_0) + \Gamma(W_L) + \Gamma(W_R)} \approx \frac{m_t^2}{2m_W^2 + m_t^2} = 70.3 \pm 0.7\%, \tag{1}$$

where the top-quark mass is $m_t = 175 \pm 3$ GeV/c^2, the W-boson mass is $m_W =$ 80.4 GeV/c^2 and the b-quark mass has been neglected. The fraction f_0 is enhanced due to the large coupling of the top quark to the Goldstone mode of the Higgs field. Fractions of left- and right-handed W bosons are denoted as f_- and f_+ respectively. In the Standard Model f_- is expected to be $\approx 30\%$ and f_+ is suppressed by a factor $(m_b/m_t)^2$, yielding at next-to-leading order a value of 3.6×10^{-4}.

The angular distribution ω of the W-boson decay products with weak isospin $I_3 = -1/2$ (charged lepton, down quark, or strange quark) in the rest frame of the W boson can be described by introducing the angle θ^* with respect to the W flight direction in the top-quark rest frame. The angular distribution has the general form

$$\omega(\theta^*) = f_0 \cdot \omega_0(\theta^*) + f_- \cdot \omega_-(\theta^*) + f_+ \cdot \omega_+(\theta^*), \tag{2}$$

with

$$\omega_0(\theta^*) = \frac{3}{4}(1 - \cos^2\theta^*), \tag{3}$$

$$\omega_-(\theta^*) = \frac{3}{8}(1 - \cos\theta^*)^2, \tag{4}$$

$$\omega_+(\theta^*) = \frac{3}{8}(1 + \cos\theta^*)^2. \tag{5}$$

Figure 1 illustrates the definition of θ^* and shows angular distributions for longitudinal, right-handed and left-handed W boson decays as well as the distribution expected in the Standard Model. For more details of the theoretical aspects of this analysis please see reference [1].

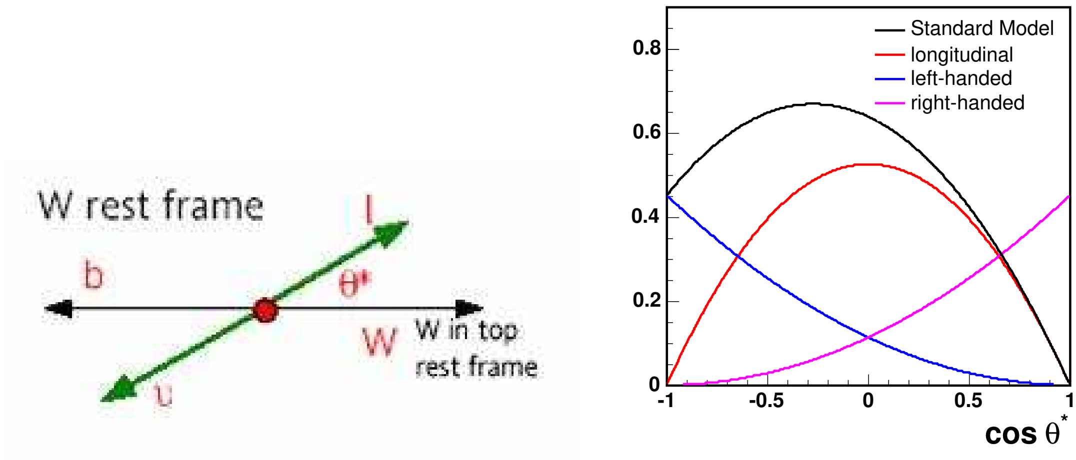

Figure 1: The decay angle θ^* in top decays is defined as the angle between the down-type particle from the W decay and the top-quark direction in the W-boson rest frame (left). The right plot shows the angular distribution $\omega(\theta^*)$ for longitudinal, right- and left-handed W-boson decays as well as the distribution expected in the Standard Model.

Due to background, reconstruction and acceptance effects the measured distribution of $\cos\theta^*$ differs from $\omega(\cos\theta^*)$. However, the shape of the observed $\cos\theta^*$ distribution depends on f_0, f_- and f_+ and can therefore be used to extract these polarization fractions. The strategy of the measurement presented here is to fully reconstruct $t\bar{t}$ events and determine the $\cos\theta^*$ distribution, and then use a template method to determine the fractions f_0, f_- and f_+.

Recent direct measurements of the longitudinal fraction by CDF and D0 have found $f_0 = 0.606 \pm 0.12 \pm 0.06$, $f_+ = -0.056 \pm 0.06 \pm 0.03$, $f_+ < 0.11 @ 95\% C.L.$ [2]; see also [3, 4], and $f_0 = 0.56 \pm 0.31$ [5] and $f_+ = 0.056 \pm 0.080(stat) \pm 0.057(syst)$, ($f_+ < 0.23$ at 95% C.L.) [5]. Measurement of $b \to s\gamma$ decay rates have indirectly limited the V + A contribution in top-quark decays to less than a few percent. However, direct measurements of the V + A contribution are still necessary because the limit from $b \to s\gamma$ assumes that electroweak penguin contributions are dominant. Direct measurements of the right-handed fraction did not find deviations from the Standard Model expectation.

2 Measurement Strategy

The strategy, performance, and systematic uncertainties are discussed in detail in the following sections. We select events with one lepton (e or μ), missing transverse energy, and at least four reconstructed jets. One of the jets has to be tagged with the tight secondary vertex tagger [7]. A cut on the scalar sum of the transverse momentum of all reconstructed objects in the event (H_T) has been applied to further reduce the background contribution. We use a kinematic fitter to find the best assignment of the top quark and its decay products to the reconstructed objects in the final state. Only the combination yielding the lowest fit chi-squared is used to reconstruct $\cos\theta^*$ from candidate events. Templates of $\cos\theta^*$ distributions for longitudinal, right- and left-handed W decays for the signal process as well as templates of $\cos\theta^*$ distributions for the background processes are reconstructed from Monte Carlo events. These distributions are parametrized and the "raw" polarization fractions F_0 and F_+ are extracted from the data using an unbinned likelihood fit. Since the selection and reconstruction efficiencies depend on the polarization of W boson, a correction is applied to obtain the true fractions, $f = F + c$, where c is determined from Monte Carlo studies and depends on the fitted fractions themselves.

2.1 Event Selection and Dataset

The final event selection is based on the $t\bar{t}$ cross section measurement described in reference [8] with missing transverse energy > 20 GeV. In order to minimize the backgrounds we require $H_T > 250$ GeV. The cut on H_T keeps 98% of the $t\bar{t}$ signal while removing about 40% of the poorly understood non-W/QCD background. Only events with at least four tight jets are used in this analysis[1]. The dataset corresponds to a total integrated luminosity of 1530 pb^{-1}. Table 1 shows the background estimate and the observed number of events. A total of 369 events satisfy the selection criteria and are used to extract the longitudinal and right-handed W-boson helicity fractions. The background numbers are scaled based on the numbers qouted in [9]. The scaled estimation of the mistag, W+H.F and the QCD background numbers is according to the ratio of the numbers of pretag events (it was also verified that this ratio goes like the ratio of luminosities). The estimation for the MC derived backgrounds - and EW processes (single top and diboson), is scaled by the luminosity. The errors in Table 1 were scaled in the same way, though when using the fitter to measure the helicity fractions we double these errors, to make sure we do not underestimate them. Inflating the errors does not have a significant effect on the fit results.

2.1.1 Signal Sample

Special $t\bar{t}$ samples, with a top mass of 175 GeV and a fixed helicity for the W decay, are used to generate the templates for the $\cos\theta^*$ distributions. A modified version of `Herwig` called `GGWIG` [15] is used to make the samples described in reference [16] except that they've been simulated and reconstructed using the 6.1.4 offline version. Data set names, sample sizes, and the acceptance for the event selection are listed in Table 2. In these GGWIG samples, which we use for creating our $\cos\theta^*$ shape templates, one of the W's is forced to decay leptonically while the other W decays with the SM branching ratios.

[1]Jets are corrected to Level-5 [14] and are required to satisfy $E_T > 20$ GeV and $|\eta| < 2$.

source	N($\geq$ 4 jet)
Mistag	9.23 ± 3.09
W+h.f.	18.02 ± 8.23
EW	6.61 ± 1.15
QCD	12.62 ± 5.05
Total	46.48 ± 17.5
Data	369

Table 1: Expected number of background events and the number of observed events using the selection criteria described in reference [9] including the $H_T >$ 250 GeV requirement and demanding at least four tight jets.

The additional $t\bar{t}$ samples used to determine systematic uncertainties are described in Section 6.

process	sample	generator	size	acceptance
W left handed $M_t = 175\ GeV$	utop0j	GGWIG	0.25M events	$0.048 \pm 5 \cdot 10^{-4}$
W right handed $M_t = 175\ GeV$	utop1j	GGWIG	0.25M events	$0.059 \pm 5 \cdot 10^{-4}$
W longitudinal $M_t = 175\ GeV$	utop2j	GGWIG	0.25M events	$0.065 \pm 5 \cdot 10^{-4}$
W left handed $M_t = 175\ GeV$	utop4j	GGWIG	0.25M events	$0.049 \pm 5 \cdot 10^{-4}$
W right handed $M_t = 175\ GeV$	utop3j	GGWIG	0.25M events	$0.59 \pm 5 \cdot 10^{-4}$
W longitudinal $M_t = 175\ GeV$	utop5j	GGWIG	0.25M events	$0.066 \pm 5 \cdot 10^{-4}$

Table 2: Summary of the Monte Carlo samples used in this analysis to model the signal. In the first three samples, the W^+ is the leptonically decaying W; in the last three, the W^- is the leptonically decaying W.

2.1.2 Background Samples

The background processes considered in the analysis are listed in Table 3 together with the data set names, total number of events, and the acceptance after all selection criteria. Our background templated is extracted from the full Alpgen reweighted evnts using all the Alpgen W+(hf)+n-parton samples.

2.2 Top-Quark Reconstruction

The top quarks are reconstructed using the same kinematic fit as used in the top mass analysis [10]. For the fit performed the mass of the top quark is unconstrained. As input to the fit the jets have their energies corrected using the top specific corrections of reference [11]. All jet-parton assignments consistent with the b-tagging information are tried and the combination which yields the lowest kinematic fit χ^2 is used. No χ^2 requirement is made. Studies using

process	sample	generator	size	acceptance
$W(e)+4p$	ptop4w	Alpgen+Pythia	1M events	$0.0035 \pm 6 \cdot 10^{-5}$
$W(\mu)+4p$	ptop9w	Alpgen+Pythia	1M events	$0.0023 \pm 5 \cdot 10^{-5}$
$W(e)+b\bar{b}+2p$	btop2w	Alpgen+Pythia	1.5M events	$0.0094 \pm 8 \cdot 10^{-5}$
$W(\mu)+b\bar{b}+2p$	btop7w	Alpgen+Pythia	1.5M events	$0.0056 \pm 6 \cdot 10^{-5}$
WW	itopww	Pythia	2.4M events	$9.33 \cdot 10^{-5} \pm 1 \cdot 10^{-5}$
WZ	itopwz	Pythia	2.4M events	$2.6 \cdot 10^{-5} \pm 4 \cdot 10^{-6}$
ZZ	itopzz	Pythia	2.4M events	$3.09 \cdot 10^{-5} \pm 4 \cdot 10^{-6}$

Table 3: Summary of the Monte Carlo samples used to model the background.

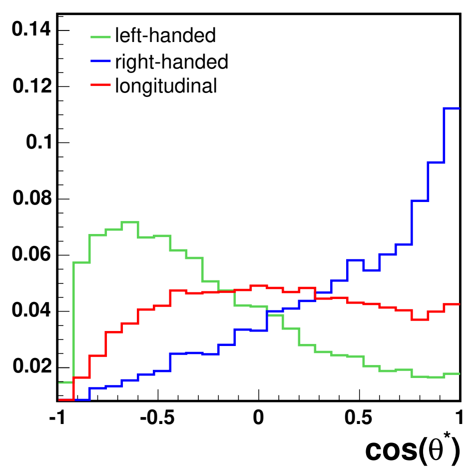

Figure 2: Reconstructed $\omega(\theta^*)$ distribution for longitudinal, right- and left-handed W boson decays (left).

pseudo-experiments indicated that there was no significant gain in statistical sensitivity from applying such a cut. The performance of the kinematic fitter was studied in a previous version of this analysis, and is described in details in reference [12].

We fully reconstruct the $\cos\theta^*$ from the four vectors of the lepton, jets and missing transverse energy returned by the kinematic fitter. Figure 2 shows the reconstructed $\omega(\theta^*)$ distribution for longitudinal, right- and left-handed W boson decays.

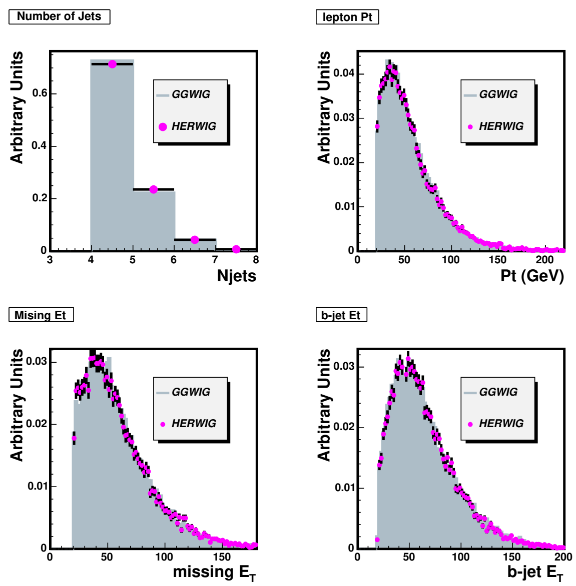

Figure 3: Comparison between events passing the event selction in Herwig (htop75) and GGWIG (mixed proportionally to SM expectation). Upper left plot - number of jets in the event, upper right - P_T of the charged lepton, lower left - missing E_T and lowe right - P_T of the jet which is tagged as a b-jet on the leptonic side of the decay.

2.3 GGWIG Validation

To validate the `GGWIG` model used in the W helicity measurement, we compare the GGWIG samples with a Pythia SM $t\bar{t}$ sample (ttop75) and with Herwig SM $t\bar{t}$ sample (htop75), all generated with a top quark mass of 175 GeV. Kinematic distributions of events passing our selection criteria are shown is Figures 3-7. There is a good agreement between data and the Monte Carlo, as well as between Pythia/Herwig and GGWIG.

2.4 Data Validation

With the good agreement we found between our GGWIG samples and other MC $t\bar{t}$ samples, we continued and validated the full data sample collected through period10 (1.53 fb^{-1} of total integrated luminosity). Validation plots of kinematic distributions comparing MC and data events passing our selection are shown in Figures 8, 9. The MC events in these plots include signal and background events. The signal is a SM mixture of GGWIG events, and the backgound expectations from Table 3.

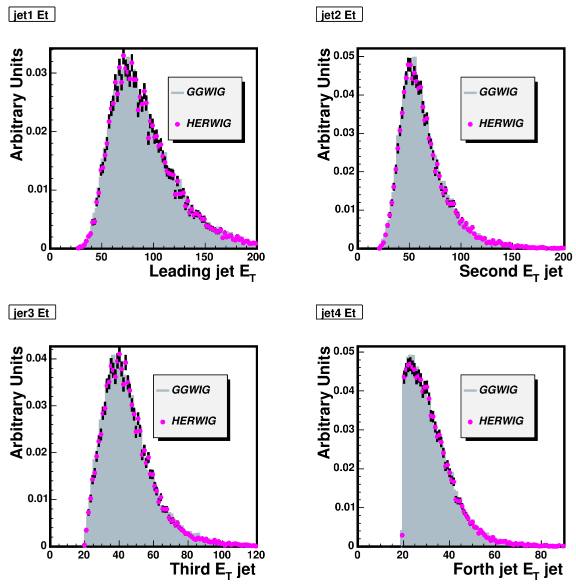

Figure 4: Jets E_T distribution for events passing the selection - comparison between Herwig (htop75) and GGWIG (mixed proportionally to SM expectation).

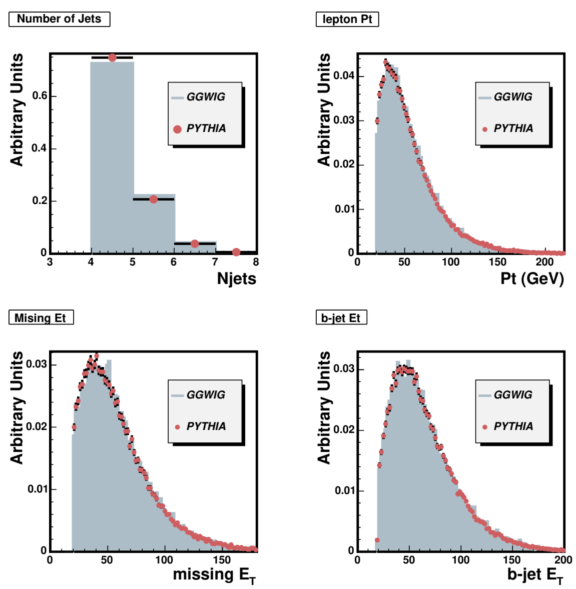

Figure 5: Comparison between events passing the event selction in Pythia (ttop75) and GGWIG (mixed proportionally to SM expectation). Upper left plot - number of jets in the event, upper right - P_T of the charged lepton, lower left - missing E_T and lowe right - P_T of the jet which is tagged as a b-jet on the leptonic side of the decay.

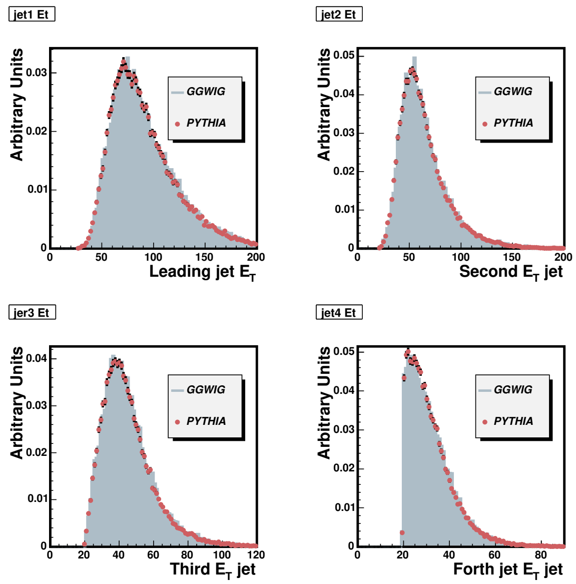

Figure 6: Jets E_T distribution for events passing the selection - comparison between Pythia (ttop75) and GGWIG (mixed proportionally to SM expectation).

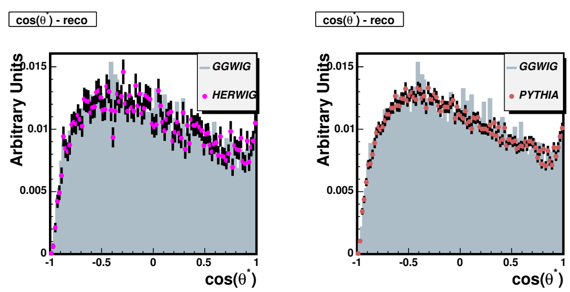

Figure 7: Comparison of the reconstructed $\cos\theta^*$ distribution in SM GGWIG mixture and SM $t\bar{t}$ Herwig and Pythia samples.

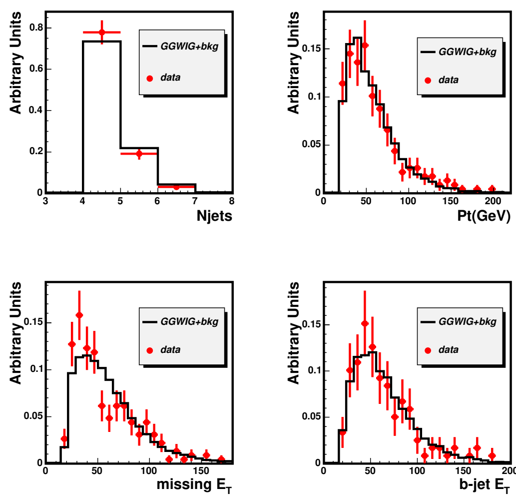

Figure 8: Comparison between events passing the event selction in data and MC (mixed proportionally to cross-section measurement with $1.12fb^{-1}$). Upper left plot - number of jets in the event, upper right - P_T of the charged lepton, lower left - missing E_T and lowe right - P_T of the jet which is tagged as a b-jet on the leptonic side of the decay.).

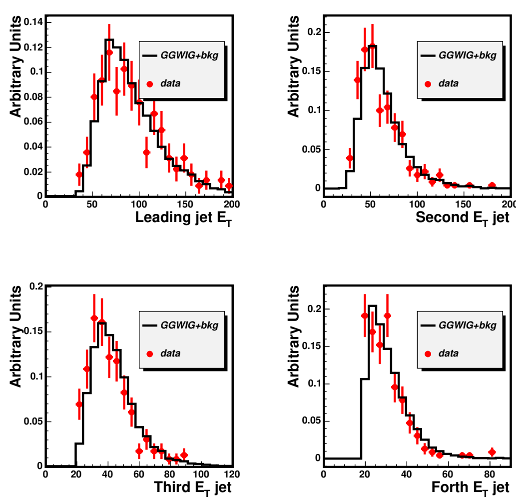

Figure 9: Jets E_T distribution for events passing the selection - comparison between data and MC (mixed proportionally to cross-section measurement with $1.12fb^{-1}$).

2.5 Fit Parameterizations of the $\cos\theta^*$ Distribution

The reconstructed $\omega(\theta^*)$ distributions for signal and background are parameterized ($\omega_{par}(\theta^*)$) using a 3rd degree polynomial times two exponential functions of the following form:

$$\omega_{par}(\theta^*) = (\sum_{i=1,2,3} p_i \cdot cos^{i-1}(\theta^*)\,) \cdot e^{p_4 \cdot cos(\theta^*)} \cdot e^{p_5 \cdot cos^2(\theta^*)}. \quad (6)$$

The fit results are summarized in Table 4. Figure 10 shows the reconstructed $\omega(\theta^*)$ distribution and the fitted parameterizations for longitudinal, right- and left-handed W-boson decays and for background. The background includes all the Alpgen W+(hf)+n-parton samples and diboson events (WW, WZ, ZZ) in their correct proportions. We use W+4jets to model the shape of the non-W background component and diboson events to model all EW processes. Figure 11 overlays the full set of parameterizations for comparison.

sample	p_1	p_2	p_3	p_4	p_5
longitudinal	-517.405 ± 60	-709.158 ± 17	635.658 ± 47	0.615 ± 0.1	0.747 ± 0.1
left-handed	-435.117 ± 23	-461.229 ± 6	480.521 ± 22	-0.126 ± 0.07	1.495 ± 0.07
right-handed	-420.181 ± 18	-466.787 ± 7	479.332 ± 15	1.788 ± 0.06	1.256 ± 0.08
background	-395.799 ± 26	-366.756 ± 12	-454.49 ± 22	0.641 ± 0.1	1.32 ± 0.02

Table 4: Summary of the resulting fit parameters used to parameterize the signal and background $\cos\theta^*$ distributions.

2.6 The Likelihood Fitter

We use an unbinned extended likelihood fitter to extract the uncorrected longitudinal and right-handed fractions, F0, and F+, from the data sample by comparing the $\cos\theta^*$ distribution for all selected events to parameterized MC templates for longitudinal, right-, and left-handed signal events, plus the parameterized background template. For a sample of N_s selected events, the likelihood function is defined as:

$$\mathcal{L} = G(b|\mu_b, \sigma_b) \cdot P(s+b|\mu_s+\mu_b) \cdot \prod_{i=1}^{N_s} (f_b p_b(\cos\theta_i^*) + (1-f_b) p_s(\cos\theta_i^*)) \quad (7)$$

and

$$p_s = F_0 \cdot p_0 + F_+ \cdot p_+ + (1 - F_0 - F_+) \cdot p_- \quad (8)$$

The term $G(b|\mu_b, \sigma_b)$ is a Gaussian constraint on b, the mean number of expected background events in the sample. The Gaussian mean, μ_b, and width, σ_b, are the a priori estimate of the background content of the lepton+jets sample as determined from Table 1. The term $P(s+b|\mu_s+\mu_b)$ is the Poisson probability that the total number of signal+background events is $s+b$ given the mean expected number of signal+background events is $\mu_s+\mu_b$. Since we use the observed cross-section as an estimate of μ_s, $\mu_s+\mu_b = Ns$. The background fraction, f_b is taken to be $b/(s+b)$. The probability density function of the background, $p_B(\cos\theta^*)$, is taken from the fit in Figure 10. Similarly for the signal, p_0, p_+, and p_- are also taken from the fits of Figure 10. In all cases the probability density functions are each required to satisfy the normalization condition $\int_{-1}^{+1} p(\cos\theta^*)\; dcos\theta^* = 1$. From equation 8 it can be seen that, at most, there are two free polarization fractions determined from the fit, F_0 and F_+. Given the limited statistics of the data sample used here, these parameters are allowed to float anywhere in the range $(-1.5, 1.5)$. As will be demonstrated in Section 3.1, this range is sufficiently wide to yield well-behaved pull distributions, even for pseudo-experiments constructed with one of the polarization fractions near the physical boundaries of 0 or 1. Since we scale the backgound numbers from $1.12fb^{-1}$ to $1.53fb^{-1}$, we double the uncertainties on the background estimation in the likelihhod fitter, to be sure we do not underestimate them. Inflating the errors does not have a significant effect on the fit results.

This fitter is the same maximum likelihood fitter used in previous versions of this analysis. Checks of the fitter were reported in [12]. This note further reports linearity checks of the fitter performance with the new parameterizations, see Section 3.1.

3 Acceptance Corrections

The kinematics of the W decay depends on its helicity. Therefore, our analysis cuts would not have the same effect on each combination of (leptonic side helicity, hadronic side helicity) of the W's in the $t\bar{t}$ decay. In order to correct for these effects when measuring the helicity fractions we have generated 3^2 different GGWIG samples. Each of these samples has a different combination of (leptonic side helicity, hadronic side helicity). We calculate the acceptance for each sample, and use it to correct the fitted values of the helicity fractions. Table 5 lists those samples and their acceptances.
The fit to the data will determine F_0 and F_+, the fraction of longitudinal and right-handed W bosons in the selected candidate sample. To extract the real fractions, an acceptance correction has to be applied. A measured helicity fraction (the value returned by the maximum likelihhod fitter) is a function of these 9 acceptances, and of the true helicity fractions in the fitted sample:

$$F_i = \frac{\sum_{j=1}^{3} f_i f_j A_{ij}}{\sum_{i,j=1}^{3} f_i f_j A_{ij}} \tag{9}$$

Here i (j) refers to the polarization of the W that decays leptonically (hadronically), F_i (f_i) refers to the measured (true) fraction, and A_{ij} is the acceptance for one of the 3^2 possible helicity configurations. For a given measured F_i, then,

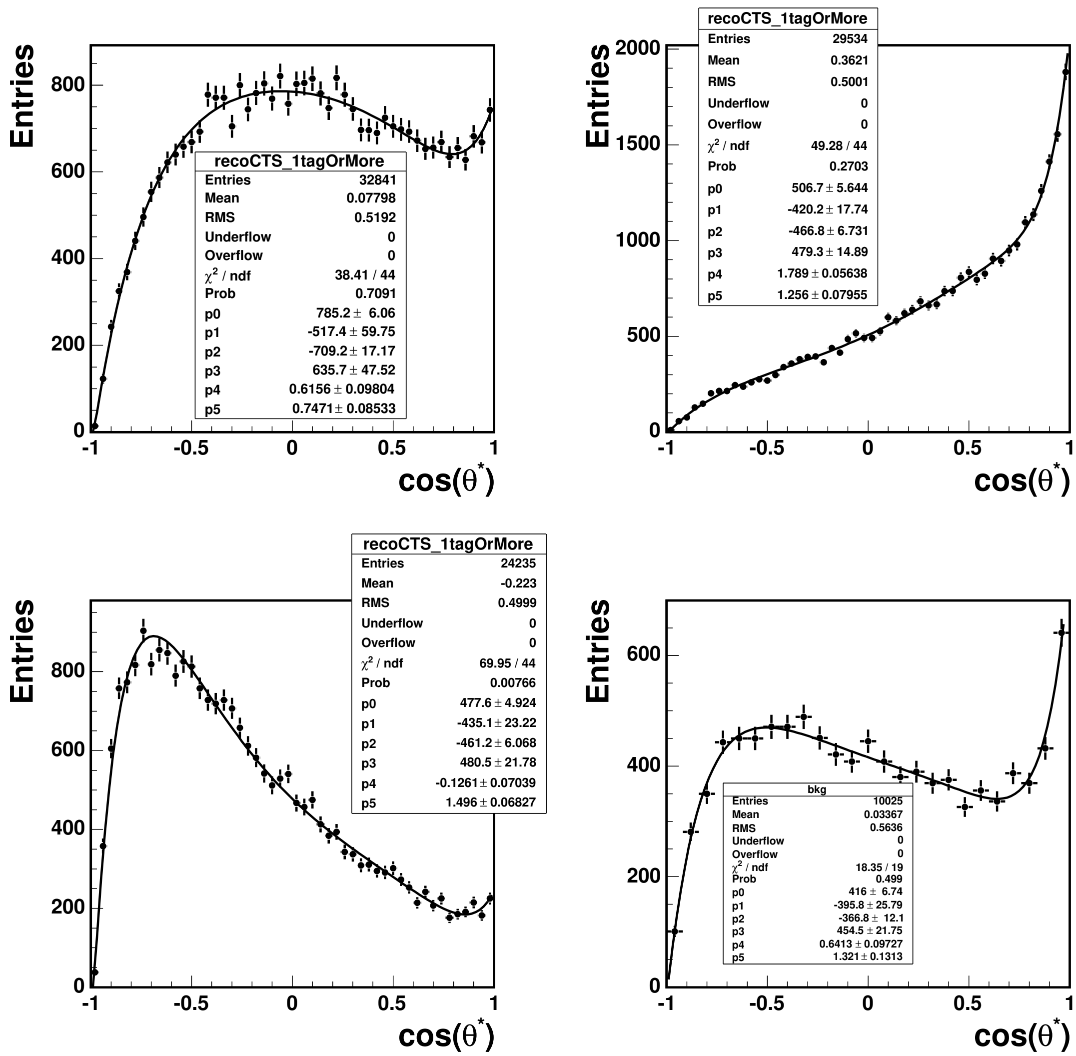

Figure 10: The reconstructed $\cos\theta^*$ distribution and the fitted parameterization for longitudinal (up-left) , right- (up-right) and left-handed (low-left) W-boson decays and for the background model (low-right).

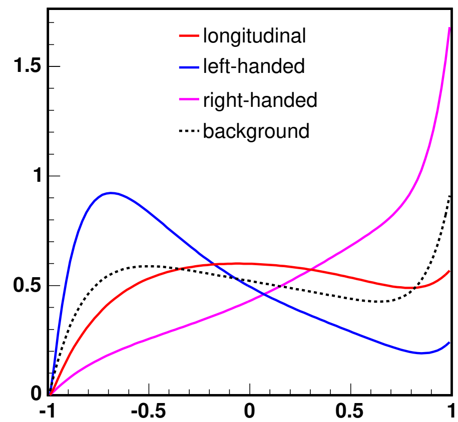

Figure 11: A comparison of the parameterizations of the reconstructed $\cos\theta^*$ distributions for signal and the dominant background sources.

we determine f_i by inverting Equation(s) 9. MINUIT is used to numerically determine the inversion.
As cross-check of the `GGWIG` samples, we verified that the acceptance of a SM GGWIG sample (utop6j) and the acceptance of Pythia $t\bar{t}$ sample (ttop75) agree. We have also verified that the actual acceptance in the different non-SM GGWIG samples (see Table 7) is deriveable from the acceptances of the individual samples listed in Table 8, see Table 6.

Now might be the appropriate time to mention that the $\cos\theta^*$ distribution for the lepton does not depend on the helicity of the hadronically decaying W (or, to be more precise, the different reconstruction efficiencies for the hadronic side helicities do not introduce a bias on the leptonic side). Recall that the signal $\cos\theta^*$ templates are constructed from GGWIG samples where all W's decay with the same helicity. We checked that same shapes are generated regardless of the helicity of the hadronic side; see Figures 12- 14.

3.1 Linearity Study and Expected Statistical Uncertainty

To test the full method, including reconstruction and acceptance effects, we generate 1000 pseudo-experiments for arbitrary values of f_0 and f_+. The mean number of background events is taken from Table 1. The number of signal events for a given pseudo-experiment is then chosen to yield 369 total events. We generate 1000 pseudo-experiments for arbitrary values of f_0, f_+, and f_-, randomly drawing from the appropriate `GGWIG` samples and mixing them in the appropriate ratios to form the signal sample. The background events are

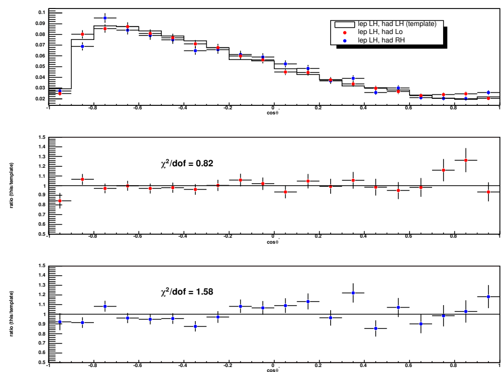

Figure 12: Top: $\cos\theta^*$ distribution for left-handed W's when the hadronic W is left-handed (template sample), longitudinal, and right-handed. Middle and bottom: Quantifying the agreement of the points with the histogram in the top plot by computing the χ^2 of their ratios bin-by-bin to a flat line at 1.

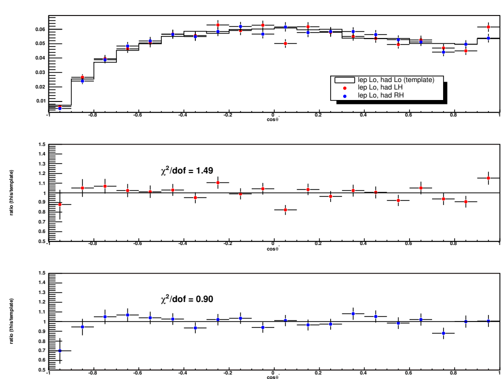

Figure 13: Top: $\cos\theta^*$ distribution for longitudinal W's when the hadronic W is longitudinal (template sample), left-handed, and right-handed. Middle and bottom: Quantifying the agreement of the points with the histogram in the top plot by computing the χ^2 of their ratios bin-by-bin to a flat line at 1.

(lep. side hel., had. side hel.)	sample	acceptance
(long, long)	utop2i+utop5i	$0.0657 \pm 5 \cdot 10^{-5}$
(long, R)	utop3k	$0.0742 \pm 8 \cdot 10^{-4}$
(long, L)	utop2k	$0.072 \pm 8 \cdot 10^{-4}$
(R, long)	utop4k	$0.0819 \pm 8 \cdot 10^{-4}$
(R, R)	utop1i+utop3i	$0.0591 \pm 5 \cdot 10^{-5}$
(R, L)	utop5k	$0.0727 \pm 8 \cdot 10^{-4}$
(L, long)	utop0k	$0.064 \pm 8 \cdot 10^{-4}$
(L, R)	utop1k	$0.057 \pm 8 \cdot 10^{-4}$
(L,L)	utop0i+utop4i	$0.0485 \pm 5 \cdot 10^{-5}$

Table 5: The acceptance as a function of the W-boson polarization determined using the $t\bar{t}$ `GGWIG` samples. These numbers are used to correct the fitted fractions $F_{0,+}$ to determine the true polarization fractions $f_{0,+}$. The uncertainties are statistical only. 'L' stands for left-handed helicity, 'R' for right-handed helicity and 'long' for longitudinal.

sample	expected weighted acceptace	actual acceptance
utop7j	0.063	$0.063 \pm 5 \cdot 10^{-4}$
utop8j	0.064	$0.064 \pm 5 \cdot 10^{-4}$
utopaj	0.066	$0.066 \pm 5 \cdot 10^{-4}$
utopbj	0.066	$0.066 \pm 5 \cdot 10^{-4}$
utopcj	0.067	$0.068 \pm 5 \cdot 10^{-4}$

Table 6: A comparison between the avarage expected acceptance in a non-SM mixture of helicity fractions and the actual acceptance in non-SM GGWIG samples (See Table 8).

randomly drawn from the $W+4p$, $W+b\bar{b}+2p$ and EW samples with the correct ratio. We find that the fit results are consistent with the input helicity fractions as shown in Table 7. In addition we generated non-SM GGWIG samples, each mixes the three W polarization with non-SM fractions. We fit each of these samples as one P.E and correct for acceptance effects. The fit results for the non-SM GGWIG samples are shown in Table 8.

Some representative pull distributions are shown in Figures 15, 16 and demonstrate that the fitter is accurately determining the statistical uncertainty. Using the pseudo- experiments constructed with the Standard Model values $(f_0, f_+) = (0.70, 0.00)$ we estimate that the expected statistical uncertainty is $\delta f_0(\text{stat}) = 0.1043$ and $\delta f_+(\text{stat}) = 0.055$ for the determination of the longitudinal and right-handed W-polarization fractions, respectively, while fixing the unmeasured fraction to its SM value. In the case of the combined fit we estimate that the statistical uncertainty is $\delta f_0(\text{stat}) = 0.24$ and $\delta f_+(\text{stat}) = 0.125$ for the determination of the longitudinal and right-handed W-polarization fractions, respectively.

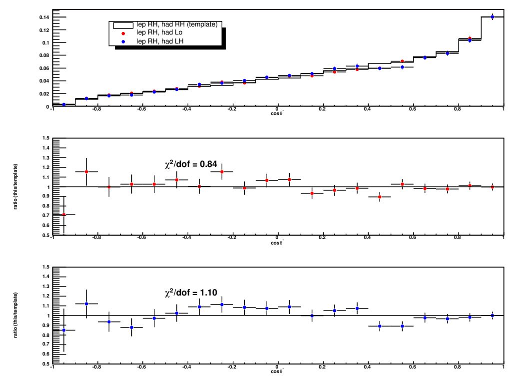

Figure 14: Top: $\cos\theta^*$ distribution for right-handed W's when the hadronic W is right-handed (template sample), longitudinal, and left-handed. Middle and bottom: Quantifying the agreement of the points with the histogram in the top plot by computing the χ^2 of their ratios bin-by-bin to a flat line at 1.

Tests of the method using pseudo-experiments in which the signal is drawn from other Monte Carlo samples (e.g. the default Pythia and Herwig $t\bar{t}$ samples) are discussed in Section 6.

MC input (f_0, f_+)	$f_0 \pm 0.02$ f_+ fixed	$f_+ \pm 0.01$ f_0 fixed	($f_0 \pm 0.04$, $f_+ \pm 0.02$) combined fit, both float
(0.3, 0.0)	0.3016	0.00035	(0.3027, -0.0008)
(0.5, 0.0)	0.4997	-0.00025	(0.4996, 0.0006)
(0.6, 0.2)	0.6022	0.202	(0.5941, 0.206)
(0.7, 0.1)	0.6995	0.1006	(0.6947, 0.104)
(0.7, 0.2)	0.7027	0.2013	(0.6923, 0.2054)
(0.8, 0.1)	0.7996	0.09945	(0.7976, 0.102)
(0.9, 0.0)	0.8997	0.0001	(0.8957, 0.0015)
(0.7, 0.0)	0.6992	$5 \cdot 10^{-5}$	(0.6934, 0.0035)

Table 7: Linearity tests of the unbinned likelihood fitter using realistic, fully simulated, signal-plus-background ensembles of 1000 Monte Carlo pseudo-experiments. Signal events are drawn from the smaples used for creating the templates (utop0j-utop5j).

4 Optimization Studies

We performed several optimization studies by generating ensembles of signal plus background pseudo-experiments for the selections listed below. In each case we tried fitting all the ≥ 1 btag events together, and treating the $== 1$ btag

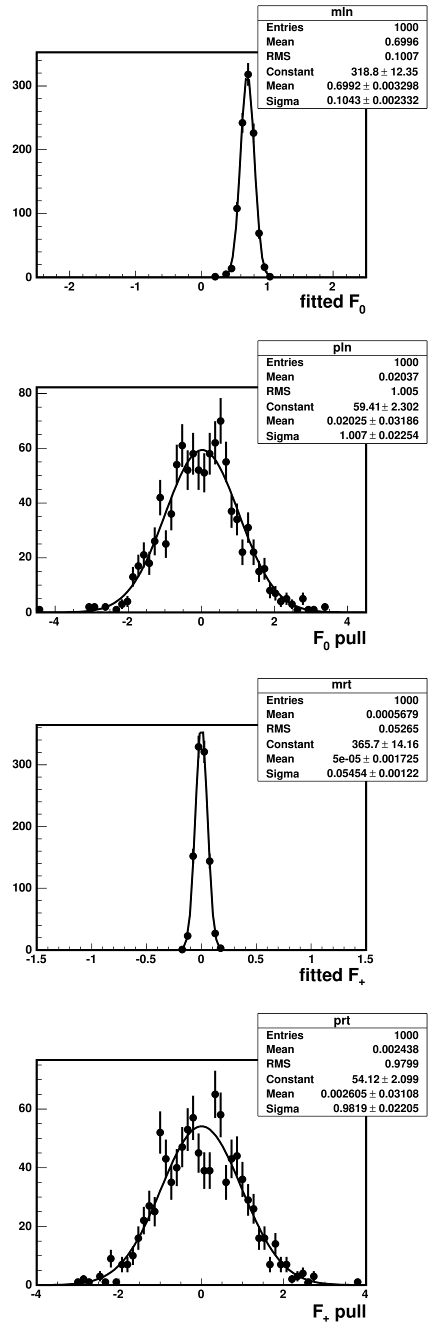

Figure 15: Representative pull distributions for the realistic signal-plus-background pseudo-experiments constructed with $(f_0, f_+) = (0.70, 0.00)$. The top two plots are the fitted f_0 and its pull when f_+ is constrained to 0. The bottom two plots are the fitted f_+ and its pull when f_0 is constrained to 0.70.

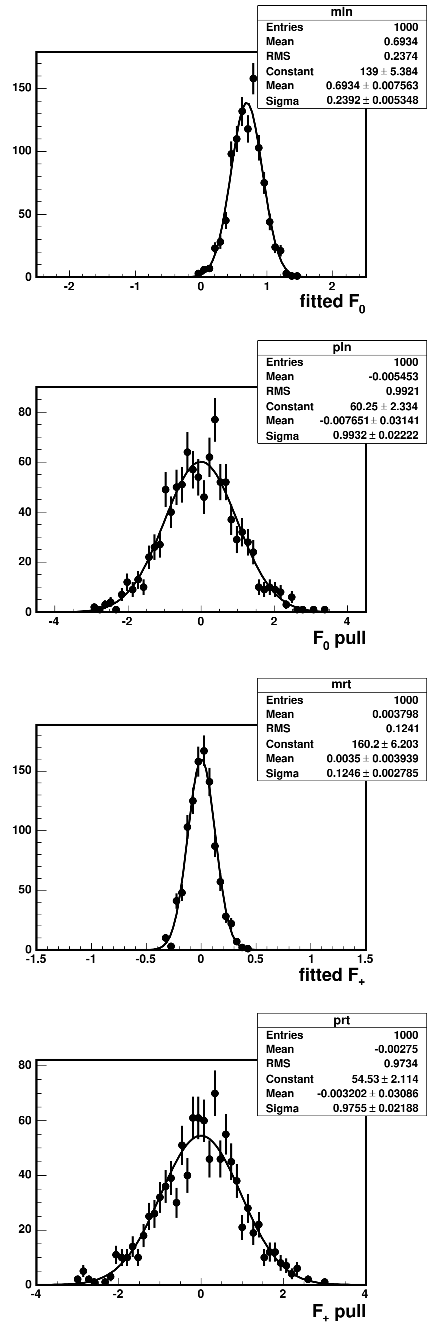

Figure 16: Representative pull distributions of the combined fit, for realistic signal-plus-background pseudo-experiments constructed with $(f_0, f_+) = (0.70, 0.00)$. The top two plots are the fitted f_0 and its pull. The bottom two plots are the fitted f_+ and its pull.

MC input (f_0, f_+), sample name	f_0 f_+ fixed	f_+ f_0 fixed	(f_0, f_+) combined fit, both float
(0.5, 0.0), utop7j	0.500 ± 0.02	0.003 ± 0.01	$(0.462 \pm 0.04,\ 0.007 \pm 0.02)$
(0.6, 0.0), utop8j	0.614 ± 0.02	0.002 ± 0.01	$(0.633 \pm 0.04,\ -0.009 \pm 0.02)$
(0.8, 0.0), utop9j	0.8024 ± 0.02	0.0106 ± 0.01	$(0.7581 \pm 0.04,\ 0.0222 \pm 0.02)$
(0.9, 0.0), utopaj	0.901 ± 0.02	0.008 ± 0.01	$(0.862 \pm 0.04,\ 0.022 \pm 0.02)$
(0.6, 0.1), utopbj	0.596 ± 0.02	0.091 ± 0.01	$(0.673 \pm 0.04,\ 0.06 \pm 0.02)$
(0.7, 0.1), utopcj	0.723 ± 0.02	0.108 ± 0.01	$(0.732 \pm 0.04,\ 0.095 \pm 0.02)$
(0.8, 0.1), utopdj	0.807 ± 0.02	0.107 ± 0.01	$(0.763 \pm 0.04,\ 0.112 \pm 0.02)$
(0.5, 0.1), utop7k	0.5061 ± 0.03	0.0908 ± 0.02	$(0.634 \pm 0.06,\ 0.0370 \pm 0.03)$
(0.9, 0.1), utop8k	0.9062 ± 0.03	0.0955 ± 0.02	$(0.983 \pm 0.05,\ 0.0548 \pm 0.03)$
(0.6, 0.2), utop9k	0.6523 ± 0.03	0.2088 ± 0.02	$(0.763 \pm 0.06,\ 0.112 \pm 0.03)$
(0.7, 0.2), utopak	0.7629 ± 0.03	0.2210 ± 0.02	$(0.8518 \pm 0.06,\ 0.167 \pm 0.04)$
(0.8, 0.2), utopbk	0.7845 ± 0.03	0.1835 ± 0.02	$(0.891 \pm 0.06,\ 0.136 \pm 0.04)$
(0.7, 0.05), utopck	0.6844 ± 0.03	0.0488 ± 0.02	$(0.627 \pm 0.06,\ 0.0793 \pm 0.03)$
(0.7, 0.0), ttop75	0.6998 ± 0.02	-0.0004 ± 0.01	$(0.7040 \pm 0.04,\ -0.0020 \pm 0.02)$

Table 8: Linearity tests of the unbinned likelihood fitter using realistic, fully simulated, signal-plus-background Monte Carlo pseudo-experiments. Signal events are drawn from the non-SM GGWIG samples. One PE using 15K events for the utop*j samples and the Pythia ttop75 sample. 7K events were used for the utop*k samples. Acceptance correction applied.

and ≥ 2 btag events separately. The $\cos\theta^*$ parameterizations were determined separately for each set of selection criteria and for the singly and doubly tagged events for signal and background. The appropriate parameterizations were included in the liklihood fit for each set of psuedo-experiments, which was modified to correctly treat the case when fitting the single and double btag events separately. The signal and background yields were estimated using the numbers from reference [9] and assuming a total luminosity of 1.2 fb^{-1}.

We find that all the variations have similar sensitivity. For simplicity we have chosen to fit the ≥ 1 btag events together. Since in the previous version of the analysis the background systematics were relatively large, we choose to use selection criteria which keep the background small. In particular we choose to use Tight SecVtx and make an H_T requirement of $H_T > 250$ GeV. The H_T cut keeps 98% of the $t\bar{t}$ selected signal events, reduces the total background by about 25%, and in particular removes 40% of the difficult to model non-W background. These requirements yield an expected signal yield of 273 events in 1.2 fb^{-1} with a purity of 85%.

We were surprised to find that dividing the sample into single and double tag events didn't yield an improved sensitivity. It's worth noting that using our selection criteria above, about 78% of the events are single tags with a purity of 86%, while the remaining 22% are double tag events with a purity of 90%. So the double tag events do not offer a substantial improvement to the purity. This

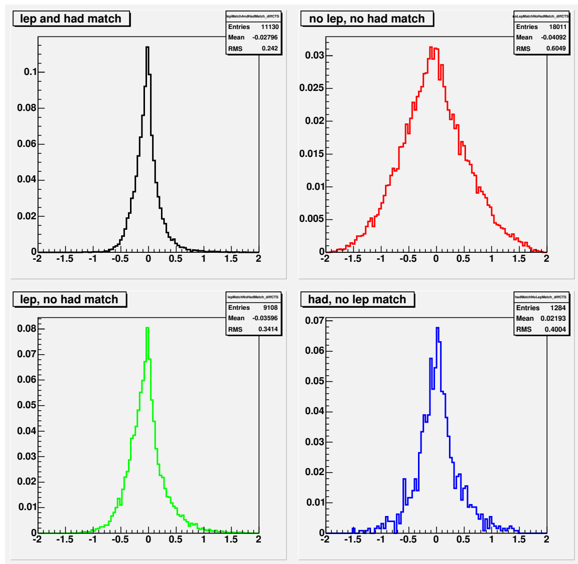

Figure 17: $\cos(\theta^*)_{reco} - \cos(\theta^*)_{hepg}$ in the four different cases of matching on the leptonic and hadronic sides of the $t\bar{t}$ decay.

is true when using Loose SecVtx as well. We also studied the $\cos\theta^*$ resolution for single and double tag events, see Figure 17. We divided our samples to four categories according to the matching between reconstruction and hepg level. One category has a match on the leptonic side but not on the hadronic side, one has a match on the hadronic side but not on the leptonic side, one has match on both sides and the last has no match on both sides. We looked at the resolutions in all those cases and calculated the averaged weighted resolution for the cases of having a sample with ≥ 1 tag, 1 tag exactly, or more than 1 tag. Table 9 summarizes the composition of each of those samples with respect to the different matching categories and gives the weighted RMSs.

sample	≥ 1 tag	==1 tag	≥ 2 tags
no match	0.45	0.48	0.37
lep and had match	0.28	0.26	0.34
lep match only	0.24	0.23	0.27
had match only	0.03	0.03	0.02
weighted resolution	0.434	0.445	0.407

Table 9: fractions of each of the four matching categories in each of the b-tags samples, and the average weighted resolution for each sample.

There's a relative improvement in resolution of about 8% between the 1 tag exactly and the ≥ 2 tags samples. However, contrary to other top properties, the mass for example, the double tag events do not offer a significant improvement to the resolution of the relevant experimental observable. From the studies above we understand this to arise from a few different effects. Firstly, the $\cos\theta^*$ resolution is less sensitive to mistakes in the jet-parton assignments of the hadronic side ($t \to Wb \to qq'b$). So while kinematic fits to double tag events do more frequently choose the correct jet-parton assignments, this doesn't translate into a significantly better resolution since it's the leptonic side which is most important. Second, the shapes of the $\cos\theta^*$ templates are more dramatically affected by acceptance biases than resolution smearing.

It should be mentioned that for Tight SecVtx tags we also tried making an H_T requirement on just the single tag events while making no H_T requirement on double tag events and then fitting them together or separately. This yielded no change in the expected sensitivity, which could be expected since the cut at 250 GeV is so efficient for the $t\bar{t}$ to begin with. We also investigated whether or not restricting ourselves to == 4 jet events would improve the sensitivity and found that it did not.

5 Results from the Data

5.1 Fitting for Longitudinal and Right-Handed Helicity Fractions Separately

We use the templates described in 2.5 to fit the observed data distribution, fixing $f_+ = 0$, to obtain $F_0 = 0.56 \pm 0.11(stat)$. After making the acceptance correction we estimate the true fraction of longitudinal polarized W-bosons to be $f_0 = 0.51 \pm 0.12(stat)$. Since the result is consistent with the Standard Model expectation, we then fit for f_+ while fixing the longitudinal fraction to the expected value assuming $m_t = 175$ GeV/c^2, $f_0 = 0.70$. We obtain $F_+ = -0.09 \pm 0.05(stat)$ and after applying the acceptance correction we find the true f_+ value to be $f_+ = -0.07 \pm 0.04(stat)$. The statistical uncertainties are reported here while the systematic uncertainties are discussed in the following sections. The $\cos\theta^*$ distributions observed in the data is hown in Figure 18. The likelihood curves for the two fits are shown in Figure 19.

5.2 Limit on f_+

As our measurement of f_+ is consistent with the SM expectation of zero, we proceed to set an upper limit on f_+ following a Bayesian prescription. We multiply the f_+ likelihood returned by the fit by a prior constant between 0 and 1 to arrive at a posterior probability density distribution for f_+, and then integrate this distribution out to the point where 95% of the area is captured; see Figure 20.

We incorporate the effect of systematic uncertainties in the determination of the limit by modeling them as a Gaussian with mean zero and width equal to the total systematic uncertainty on f_+ (see Sec. 6). We have verified that the

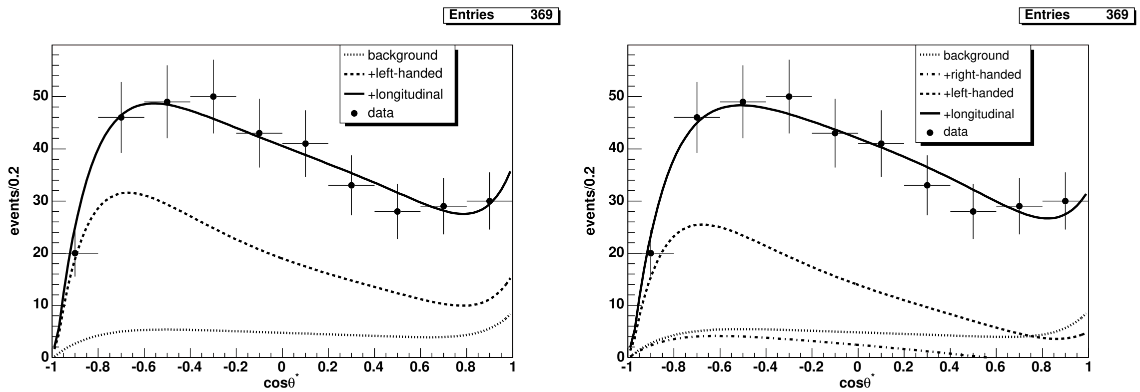

Figure 18: The observed $\cos\theta^*$ distribution in the data (points) overlaid with the background (dotted), background + left-handed (dashed), and background + left-handed + longitudinal (solid) distributions as determined by the fit for F_0 (on the left) nd for F_+ (on the right).

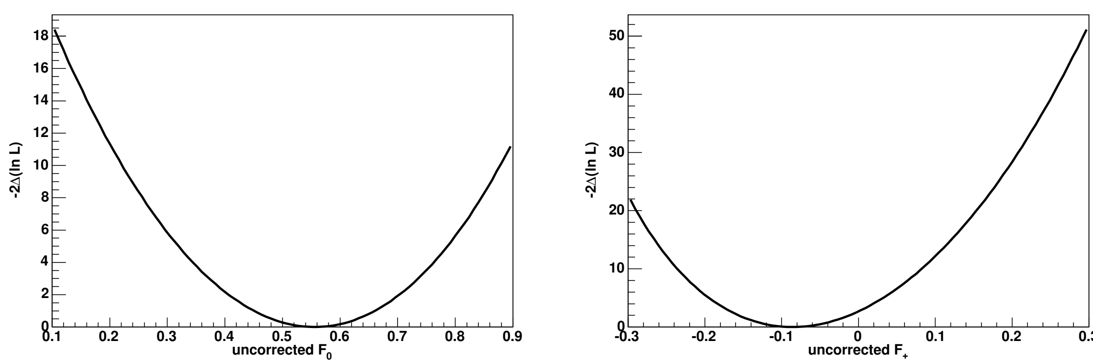

Figure 19: Distributions of $-2\Delta\ln\mathcal{L}$ for F_0 (left plot) and F_+ (right plot) from the fits to the data.

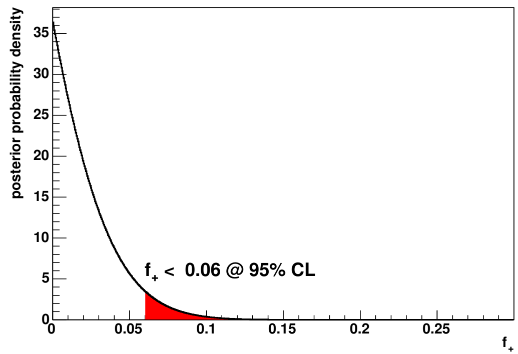

Figure 20: Posterior probability distribution for and 95% CL upper limit on f_+.

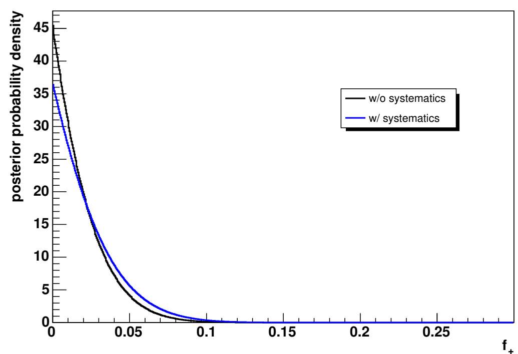

Figure 21: f_+ posterior probability with (blue) and without (black) folding in systematic uncertainties.

systematic uncertainties on f_+ reported in Table 11 are independent of the f_+ value used in the pseudo-experiments used to quantify them.

We then convolute the f_+ likelihood with this Gaussian before multiplying by the prior. Since the total f_+ uncertainty is still statistics dominated, the systematics have only a very small effect on the posterior probability distribution; see Figure 21. The 95% CL upper limit on f_+ determined from this procedure is 0.06.

5.3 Fitting for Longitudinal and Right-Handed Helicity Fractions Simultaneously

We perform a fit to the data to extract both the fraction of longitudinal and right-handed polarized W bosons. We obtain $F_0 = 0.63 \pm 0.24(stat)$ and $F_+ = -0.04 \pm 0.12(stat)$.

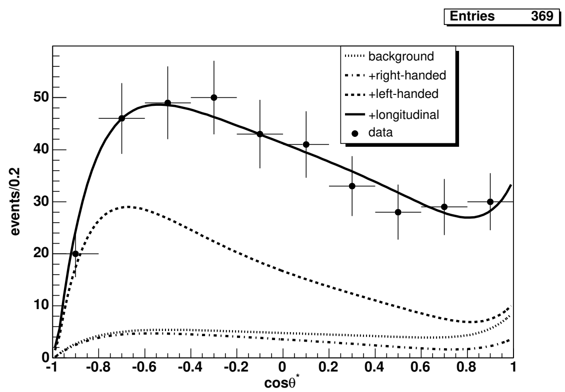

Figure 22: The observed $\cos\theta^*$ distribution in the data (points) overlaid with the background (dotted),background + right-handed (dash-dot), background + right-handed + left-handed (dashed), and background + right-handed + left-handed + longitudinal (solid) distributions as determined by the fit for F_+.

After correcting for acceptance effects, we estimate the true fraction of longitudinal polarized W bosons to be $f_0 = 0.58 \pm 0.24(stat)$ and $f_+ = -0.04 \pm 0.10(stat)$. The fit to the data is shown in Figure 22. Only the statistical uncertainties are reported here while the systematic uncertainties are discussed in the following sections.

The likelihood as a function of f_+ and f_0 is shown in Figure 23. We construct a posterior probability density in the (f_+, f_0) plane by multiplying the likelihood by a prior that is flat in the physical region defined by $f_+ \geq 0$, $f_0 \geq 0$, $f_0 + f_+ \leq 1$ and is zero everywhere else. We then set an exclusion at 95% CL in this plane by finding the contour of constant probability density that captures 95% of the volume under the probability surface. This is shown in Figure 24. This procedure does not explicitly incorporate the effects of the systematic uncertainties on f_+ and f_0; however, the fact that the systematics are about a factor of four less than the statistical uncertainties (see Section 6) renders their contribution to the exclusion limit negligible.

6 Systematic Uncertainties

Aside from the statistical uncertainty on the measurement which arises due to the finite size of the data sample, the systematic uncertainties associated with the measurement of f_0 and f_+ must also be considered. In almost all cases the systematic uncertainty was determined by constructing pseudo-experiments with signal and/or background templates affected by the systematic under study but fit using the default parameterizations and normalizations described above. The resulting shifts in the mean fitted longitudinal and right-handed fraction are used to quantify the systematic uncertainty. The pseudo-experiments were

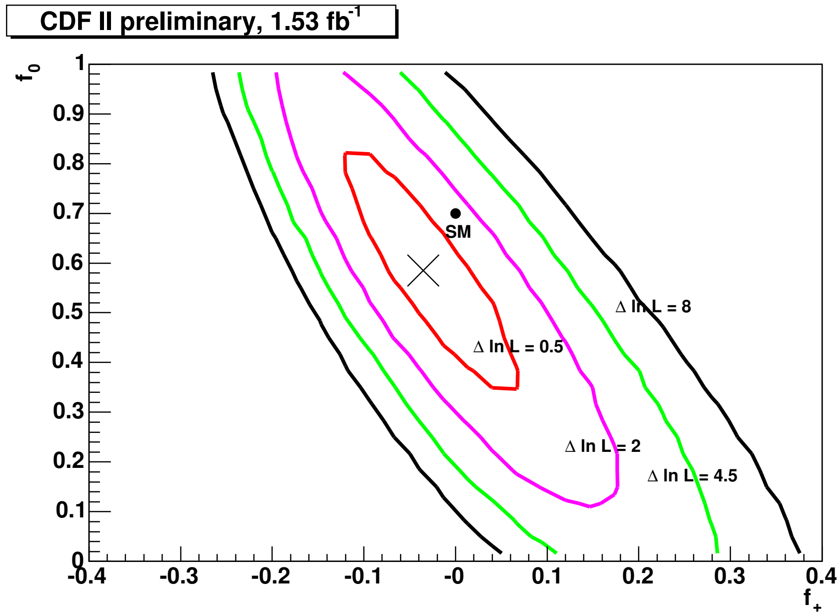

Figure 23: Contours of constant ln-likelihood in the (f_+, f_0) plane from the fit to the data. The X shows the minimum of the ln-likelihood, *i.e.* our result.

all performed using the default Pythia sample (`ttop75`) as signal, which has the Standard Model values $(f_0, f_+) = (0.70, 0.00)$, and our background model as described in Sec. 2.1.2 unless otherwise noted. The following sources of systematic uncertainties have been considered:

- Jet Energy Scale
- Background
- Initial State Radiation
- Final State Radiation
- Parton Distribution Functions
- Monte Carlo Modeling

These are each discussed in more detail in the following sections.

6.1 Jet Energy Scale

Changes in the Jet Energy Scale (JES) have two effects on the analysis. They can change the acceptance and the $\cos\theta^*$ shapes. We investigate each of these separately. First, we re-evaluate the acceptances for `GGWIG` samples when we

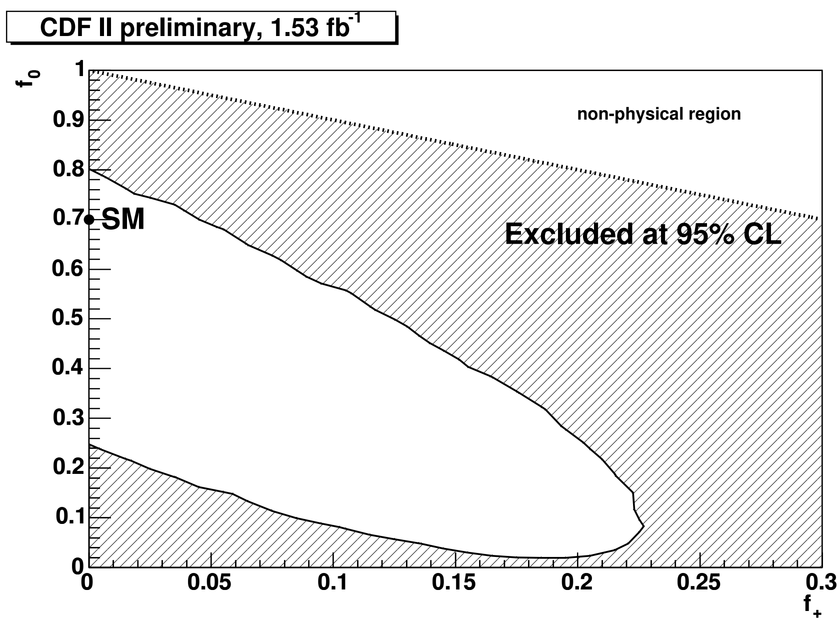

Figure 24: The area of the (f_+, f_0) plane excluded by the data is shown as the hatched region (do you have anti-aliasing switched off?) The unhatched region in the upper right is unphysical.

vary the JES by $\pm 1\sigma$ and propagate those changes into the acceptance correction. The resulting change in the correction is $<< 0.01$ and is neglected. Second, we construct pseudo-experiments in which the signal and background are constructed from events reconstructed with $\pm 1\sigma$ shifts in their jet energies. The difference between the mean fitted values of f_0 (f_+) from pseudo-experiments where the GGWIG samples JES is varied by $+\sigma$ and $-\sigma$ are calculated. This difference is taken to be the JES systematics for f_0 (f_+). We find these uncertainties to be ± 0.013 for f_0 and ± 0.010 for f_+.
In the case of the combined fit we find these uncertainties to be exactly the same.

6.2 Background

Uncertainties in the background normalization are already accounted for in the fit by inclusion of the Gaussian constraint. Remaining sources for systematic uncertainties are the background sample composition and the uncertainty of the shape for each sample.

For simplicity, our background model uses events from the samples listed in Table 3, as they account for most of the background statictics. To assess the uncertainty due to the background model shape and the backgound composition we construct different sets of pseudo-experiments, varying the background composition of each of these sets. Table 10 shows the mean fitted values for pseudo-experiments with different background compositions. Even the more extreme variations listed in the bottom 3 rows of Table 10 yield differences of $< 5\%$, indicating that the method is fairly insensitive to the details of the background modeling. From the mean values returned by the fitter shown in this table we conclude that a reasonable variation of the background composition gives an uncertainty of about 1% for measuring f_+ while f_0 is fixed to 0.7, and uncertainties od about 2% for measuring f_0 while f_+ is fixed to 0. In the case of the combined fit we assign an uncertainty of 2% for the measurement of the two fractions.

W+jets MC events have been used to model the shape of QCD background shape. To gain confidence in the background model, an anti-electrons sample has been studied, in which electron are fakes by light flavour jets. The sample was used and added with a background fraction of 28% to the total background samples. Pseudo-experiments show a systematic uncertainty of ± 0.023 and ± 0.015 for f_0 and f_+, respectively when doing the standard fit. For the combined fit we estimate these uncertainties to be ± 0.01 and ± 0.015 for f_0 and f_+, respectively . Figure 25 shows the $\cos\theta^*$ distribution for the anti-electrons sample.

Adding in quadrature a the uncertainties due to the background composition modeling, and the undertainties from mixing anti-electrons events as the QCD component of the background, results in a total background systematic uncertainty of ± 0.02 for measuring f_+ while f_0 is fixed, and ± 0.03 for measuring f_0 while f_+ is fixed as well as for measuring f_0 and f_+ simultaneously.

Further tests have been performed to show the agreement of the background model with the data. Using event without b-tag, we create a sample dominated

Background composition	$f_0 \pm 0.02$ f_+ fixed	$f_+ \pm 0.01$ f_0 fixed	$(f_0 \pm 0.04,\ f_+ \pm 0.02)$ combined fit, both float
$2\sigma(W+bb)$	0.7042	0.00265	(0.6991, 0.00245)
$2\sigma(W+4p)$	0.7168	0.01085	(0.6823, 0.0195)
$2\sigma(EW)$	0.7041	0.0031	(0.695, 0.007)
default	0.7088	0.00645	(0.6893, 0.01215)
all=W+4p	0.7247	0.0165	(0.677, 0.0271)
all=W+$b\bar{b}$	0.7034	0.001	(0.7079, 0.00245)
flat	0.6705	-0.0137	(0.6647, 0.00295)

Table 10: Fitted values from sets of 1000 PE mixing GGWIG in the SM proportion and varying the background composition. The default background is based on the background estimation for $1.12 fb^{-1}$ [9]. The 2σ rows show the fitted values when changing one of the background components by 2σ while keeping the total number of background events unchanged and the ratio betwwen the other background components according to Table 1

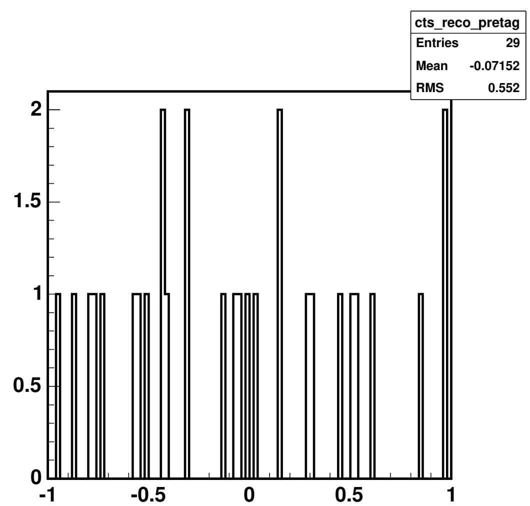

Figure 25: The $\cos\theta^*$ distribution for the anti-electron sample.

by W+jets and QCD events. The $\cos\theta^*$ distribution is shown in Figure 26. This sample shows a good agreement with our background model, which gives us confidence that it is a reasonable description of the background in the signal region.

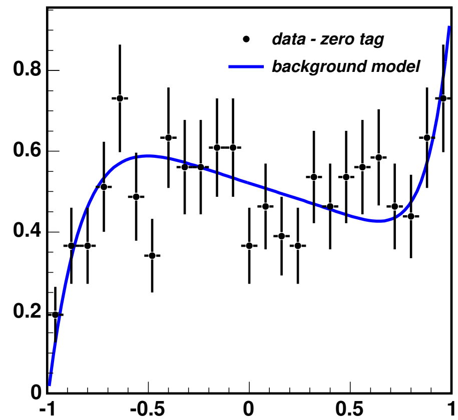

Figure 26: $\cos\theta^*$ distribution in the zero-tag sample is shown, together with the background model.

6.3 Initial and Final State Radiation

We compare the mean fitted f_0 and f_+ when using the ISR (FSR) more/less samples, `itoprk` and `itoprl` (`ftoprj` and `ftoprl`), for the signal events in pseudo-experiments. We take the full difference between these two samples as the systematic uncertainty, ±0.01 and ±0.002 for f_0 and f_+, respectively. For the simultaneous fit we find these uncertainties to be ±0.01 and ±0.02 for f_0 and f_+, respectively.

6.4 Signal Monte Carlo

We construct pseudo-experiments using events from the default Pythia sample (`ttop75`) as signal and compare the mean fitted f_0 and f_+ to the mean fitted values when using the default Herwig sample (`htop75`) for the signal events. We take the full observed difference as a systematic uncertainty of ±0.02 and ±0.01 for f_0 and f_+, respectively.
For the simultaneous fit of f_0 and f_+ we find these uncertainties to be 0.01 in both cases.

6.5 Parton Distribution Functions

The effect of PDFs is studied using the re-weighting technique [18]. The PDF we used are:

- CTEQ5L - the default PDF. The relative weight for every event is 1.
- MRST72 - Leading order PDF. If a difference relative to the default PDF is found it should be taken as a systematic.
- MRST75 - Same as the previous, but using a different value of α_s, corresponding to $\Lambda_{QCD} = 300\ MeV$ vs. $\Lambda_{QCD} = 228\ MeV$ for MRST72. The difference between the two PDFs is taken as a systematic.

In order to assign a systematic uncertainty due to differences between the MRST72 PDF and the default CTEQ5L PDF we fit the reweighted Pythia $t\bar{t}$ sample (ttop75). The difference between the fitted values we get from the weighted sample and the default unweighted sample is taken as a systematic uncertainty. It is found to be ± 0.0008 for all fits, same fot the MRST75 uncertainties.

Another source for a PDF related systematic uncertainty are the variations of the 20 CTEQ6M eigen-vectors. The sample is reweightes according to variations of $\pm 1\sigma$ of each of the eigenvectors separately.

We plot 40 different re-weighted histograms of $\cos\theta^*$ corresponding to $\pm 1\sigma$ variation of the 20 free PDF parameters in the CTEQ6 global PDF fit. For each event we normalize the weights of the 40 CTEQ6M variations with respect to the weight we get from the CTEQ5L PDF. We apply our fitter to extract the W-helicity fractions for each variation. A systematic uncertainty for f_+ and f_0 is assigned [20]:

$$\Delta F = \frac{1}{2}(\sum_{i=1}^{20}[F(S_i^+) - F(S_i^-)]^2)^{1/2} \tag{10}$$

Where F is either f_+ or f_0 and $F(S_i^{\pm})$ are the values correspond to $\pm 1\sigma$ variation of the 20 eigen-vectors returned by the fitter. This yields uncertainties of ± 0.005 for both f_0 and f_+. In the case of the combined fit, we estimate these uncertainties to be ± 0.005 and ± 0.002 for f_0 and f_+ respectively.

6.6 Method

- In previous versions of this analysis, using Gen5, we propagated the statistical uncertainty on the GGWIG acceptances to an uncertainty on the acceptance correction. This uncertainty was estimated to be about 1%. Having about 100 times more of the statistics for the GGWIG samples now, the uncertainty on the acceptances of the GGWIG smaples is of the order 10^{-5} and has no effect when propagated to an uncertainty on the acceptance correction or on the fitted helicity fractions.

- The number of reconstructed vertices is different between data and MC. We fit two samples - one contains 10000 GGWIG events with 2 reconstructed vertices or less, the other one contains 2000 events with 3 reconstructed vertices or more. The fits to these two samples are in agreement within their uncertainties. Therefore, although data and MC are not in good agreement for the number of reconstructed vertices, we do not expect it to be a problem in our fit, and do not assign a systematic uncertainty for that.

6.7 Summary of Systematic Uncertainties

The systematic uncertainties from each of the sources given above are summarized in Table 11. The total systematic uncertainty is taken to be their quadrature sum.

source	δf_0 f_+ fixed	δf_+ f_0 fixed	δf_0 combined fit	δf_+ combined fit
Jet Energy Scale	± 0.013	± 0.01	0.013	0.01
Background	± 0.03	± 0.02	0.03	0.03
ISR	± 0.005	± 0.0001	0.005	0.001
FSR	± 0.005	± 0.0001	0.005	0.001
Signal Monte Carlo	± 0.020	± 0.01	0.01	0.01
PDF	± 0.005	± 0.005	0.005	0.002
Total Systematic	± 0.04	± 0.025	0.036	0.034
Statistical	± 0.101	± 0.053	0.24	0.124
Total Uncertainty	± 0.109	± 0.059	0.24	0.13

Table 11: The sources of systematic uncertainty and their related estimate. The total systematic uncertainty is taken as the quadrature sum of the individual sources.

7 Conclusions

We use a sample of fully reconstructed $t\bar{t}$ events to determine the W-boson helicity fractions. Using an unbinned liklihood fit and fixing the right-handed fraction to zero we measure fraction of longitudinally polarized W-bosons to be

$$f_0 = 0.51 \pm 0.12\,(\text{stat}) \ \pm 0.04\,(\text{syst}). \tag{11}$$

This is consistent with the Standard Model expectation of $f_0 = 0.70$. Using the same fit but fixing the longitudinal fraction to it's Standard Model expectation we measure the fraction of right-handed polarized W-bosons to be

$$f_+ = -0.07 \pm 0.04\,(\text{stat}) \ \pm 0.025\,(\text{syst}) \tag{12}$$

$$f_+ < 0.06 \text{ at } 95\%\text{CL}, \tag{13}$$

Fitting for the longitudinal and right-handed helicity fractions simultaneously, we obtain:

$$f_0 \quad = \quad 0.58 \pm 0.24\,(\text{stat}) \;\; \pm 0.036\,(\text{syst}) \tag{14}$$

$$f_0 \quad = \quad -0.04 \pm 0.10\,(\text{stat}) \;\; \pm 0.034\,(\text{syst}) \tag{15}$$

A measurement of f_+ significantly different from zero would be evidence of new physics.

References

[1] CDF internal note 8637.

[2] CDF internal note 8368.

[3] CDF internal note 8380

[4] CDF note 8229; CDF note 8250.

[5] V.M. Abazov, *et al.*, (DØ Collaboration), *Phys. Lett. B* **617**, 1 (2005).

[6] Measurement of the W boson helicity in top quark decay at D0, (DØ Collaboration), http://arxiv.org/abs/hep-ex/0609045.

[7] W.Yao, *et al.*, "A Seed Vertexing Algorithm for Top", CDF note 2716; D. Glenzinski, *et al.*, "A Detailed Study of the SECVTX Algorithm", CDF note 2925; C. Neu, itet al., "SecVtx Optimization Studies for 5.3.3 Analyses", CDF note 7578; C. Rott, itet al., "SecVtx Optimization for the 2003 Winter Conferences", CDF note 6242.

[8] Measurement of the Top Pair Production Cross Section in the Lepton+Jets Decay Channel, CDF internal note 8795.

[9] "Method 2 Backgrounds for 1.12/fb Lepton+Jets Analyses", CDF internal note 8766.

[10] A. Abulencia, *et al.*, (CDF Collaboration), *Phys. Rev.* **D 73**, 032003 (2006).

[11] J.-F. Arguin and P.K. Sinervo, "Revisiting the Top-Specific Jet Energy Corrections", CDF note 6404.

[12] CDF internal note 8230.

[13] S. Budd, *et al.*, "Measurement of the t-tbar Production Cross Section in SecVtx-Tagged Lepton+Jets Events", CDF note 8037.

[14] F. Canelli, and A. Bhatti, "Generic Jet Corrections for Run II", CDF note 7358; see also `http://www-cdf.fnal.gov/internal/physics/top/jets/corrections.html`.

[15] G. Guillian, M. Campbell, D. Amidei, "A Modified Version of HERWIG for Studying the Spin Properties of the Top Quark", CDF note 4261.

[16] N. Goldschmidt, *et al.*, "Measurement of the Fraction of Longitudinally Polarized W-Bosons Produced in Top-Quark Decays", CDF note 6950.

[17] Tevatron Electroweak Working Group, "Combination of CDF and DØ Results on the Top-Quark Mass", Fermilab-TM-2323-E, (`hep-ex/0507091`).

[18] see `http://www-cdf.fnal.gov/internal/physics/top/run2mass/topmass_systematics.html`

[19] J. Huston "PDF uncertainties and their meaning", talk at Joint physics meeting May 5, 2006

[20] J. Pumplin, D.R Stump, J. Huston, H.L. Lai, P. Nadolsky, W.K Tung "New Generation of Parton Distributions with Uncertainties from Global QCD Analysis", hep-ph/0201195